ELSEVIER

MRI based diffusion and perfusion predictive model to estimate stroke evolution

Stephen E. Rose[a,*], Jonathan B. Chalk[a,b], Mark P. Griffin[a], Andrew L. Janke[a], Fang Chen[e],
Geoffrey J. McLachan[c], David Peel[c], Fernando O. Zelaya[g], Hugh S. Markus[h]
, Derek K. Jones[f,i], Andrew Simmons[f], Michael O'Sullivan[h], Jo M. Jarosz[f],
Wendy Strugnell[d], David M. Doddrell[a], James Semple[j]

[a]*Centre For Magnetic Resonance, University of Queensland, Brisbane, Queensland 4072, Australia*
[b]*Department of Medicine, University of Queensland, Brisbane, Queensland 4072, Australia*
[c]*Department of Mathematics, University of Queensland, Brisbane, Queensland 4072, Australia*
[d]*Department of Radiology, Princess Alexandra Hospital, Brisbane, Australia*
[e]*Brain Research Institute, Melbourne, Australia*
[f]*Neuroimaging, King's Healthcare, St George's Hospital Medical School London, UK*
[g]*Neuroimaging Institute of Psychiatry, De Crespigny Park, London, UK*
[h]*Clinical Neuroscience, St George's Hospital Medical School London, UK*
[i]*Divison of Medical Physics, Leicester Royal Infirmary, Leicester, UK*
[j]*GlaxoSmithKline Pharmaceuticals, Addenbrooke's Centre for Clinical Investigation, Cambridge, UK.*

Abstract

In this study we present a novel automated strategy for predicting infarct evolution, based on MR diffusion and perfusion images acquired in the acute stage of stroke. The validity of this methodology was tested on novel patient data including data acquired from an independent stroke clinic. Regions-of-interest (ROIs) defining the initial diffusion lesion and tissue with abnormal hemodynamic function as defined by the mean transit time (MTT) abnormality were automatically extracted from DWI/PI maps. Quantitative measures of cerebral blood flow (CBF) and volume (CBV) along with ratio measures defined relative to the contralateral hemisphere (r_aCBF and r_aCBV) were calculated for the MTT ROIs. A parametric normal classifier algorithm incorporating these measures was used to predict infarct growth. The mean r_aCBF and r_aCBV values for eventually infarcted MTT tissue were 0.70 ± 0.19 and 1.20 ± 0.36. For recovered tissue the mean values were 0.99 ± 0.25 and 1.87 ± 0.71, respectively. There was a significant difference between these two regions for both measures ($p < 0.003$ and $p < 0.001$, respectively). Mean absolute measures of CBF (ml/100g/min) and CBV (ml/100g) for the total infarcted territory were 33.9 ± 9.7 and 4.2 ± 1.9. For recovered MTT tissue, the mean values were 41.5 ± 7.2 and 5.3 ± 1.2, respectively. A significant difference was also found for these regions ($p < 0.009$ and $p < 0.036$, respectively). The mean measures of sensitivity, specificity, positive and negative predictive values for modeling infarct evolution for the validation patient data were 0.72 ± 0.05, 0.97 ± 0.02, 0.68 ± 0.07 and 0.97 ± 0.02. We propose that this automated strategy may allow possible guided therapeutic intervention to stroke patients and evaluation of efficacy of novel stroke compounds in clinical drug trials. © 2001 Elsevier Science Inc. All rights reserved.

Keywords: Acute stroke; Magnetic resonance imaging; Diffusion and perfusion

1. Introduction

In contrast to conventional T_2-weighted MRI, diffusion-weighted (DWI) echoplanar MRI can identify ischemic brain tissue in acute stroke patients (1–5). The DWI lesion is normally defined as tissue with a reduced measure of the apparent diffusion coefficient of water (ADC). Changes in the effective diffusivity of water occur when there is a disruption of oxygen-dependent high energy Na-K ATPase ionic pumps. These ionic pumps regulate cellular ionic gradients that maintain neuronal integrity [6–8]. Diffusion tensor imaging (DTI), a form of DWI, can be used to

---

* Corresponding author. Tel.: +1-617-33654237; fax: +1-617-33653833.
E-mail address: Stephen.Rose@cmr.uq.edu.au (S. Rose).

identify ischemic brain tissue [9–11]. As DTI allows computation of all elements of the water diffusion tensor, a measure of infarct volume free from orientational artifacts, can be obtained.

MR perfusion imaging (PI) using dynamic susceptibility contrast enables the identification and characterization of perfusion deficits both within and importantly in regions surrounding the ischemic core [12–16]. Perturbations in perfusion can be analyzed from maps of cerebral blood flow (CBF), cerebral blood volume (CBV) and mean transit time of the bolus passage of the contrast agent (MTT) through an ischemic region. Quantitation of these perfusion parameters measured with MRI has found to be consistent with those obtained using PET [17,18]. The mismatch between the abnormalities delineated on the initial perfusion and diffusion maps acquired in the acute stage of stroke has previously been reported to represent the ischemic penumbra [2,13–16,20,21]. The recently demonstrated reversibility of the diffusion lesion with thrombolytic therapy has enabled redefinition of the ischemic penumbra to include both the diffusion–perfusion mismatch and regions of the initial diffusion abnormality [22]. The magnitude of the DWI/PI mismatch has been shown to correlate with neurologic impairment scores and infarct size measured on follow-up T_2-weighted MRI [13,14]. However, even though the diffusion lesion normally expands into the surrounding hypoperfused penumbra, a model of infarct evolution based on this simple mismatch parameter alone does not accurately predict the final infarct volume [2,13,20,21]. Never the less, attempts have been made to model perfusion parameters in the ischemic penumbra [23] and predict infarct evolution [24]. To date, previous studies have relied on the use of subjective measures such as operator defined regions-of-interest (ROIs) on DWI or PI maps to predict infarct size. However these methods are time consuming to implement and there is a limited time window of opportunity for the administration of thrombolytic or neuroprotective therapy [25]. Thus a basic criterion for a predictive model-based prognostic aid in the acute stroke clinic is that the method is both rapid and automated.

In this study we wish to present results from a novel automated method for predicting infarct evolution. The method comprises two parts. (i) The calculation of diffusion and perfusion measures within the MTT region of abnormal flow and (ii) utilization of these metrics in a parametric normal classifier algorithm [26] to predict infarct growth. Although this methodology allows automated measurement of the diffusion lesion and perfusion mismatch, modeling diffusion and perfusion measures within the MTT abnormality circumvents any a priori definition of an ischemic penumbra. The validity of this methodology was tested on novel patient data including data acquired from an independent stroke clinic.

2. Materials and methods

2.1. Patients

Nineteen patients (9 male and 10 female, age 75.6 ± 9.1) with acute focal neurologic symptoms consistent with hemispheric ischemic stroke and radiographic evidence of a diffusion-perfusion mismatch were recruited into this study. In this group of patients, the diffusion lesion normally expands into the surrounding hypoperfused territory [5,16]. Five patients data (13–17) was acquired from an independent stroke clinic. Approval to carry out the study was obtained from the Human Experimental Ethics Committees of both institutions. The "time of first scan" was defined as the time elapsed between the initial MRI scans and the last time the patient was known to be without neurologic deficit. The mean "time of first scan" was 8.9 (±3.5) hours. Five patients (9–12,16) were scanned within the six-hour window where therapeutic intervention is normally contemplated. Patients were excluded if they had cerebral hemorrhage or some other preexisting nonischemic neurologic condition that would confound clinical or MR assessment. Patients enrolled in this study received serial DWI and PI examinations. For each patient the last MRI scan was used to determine the final lesion volume. The mean last follow-up examination time was 818 (± 674) hours. Three patients (1,10,12) died within seven days of onset of symptoms. In these patients, the presence of edema may result in an overestimation of final lesion volume [21]. Patients who were treated with recombinant tissue plasminogen activator or any neuroprotective therapy were excluded from the study.

2.2. Imaging protocol

In the acute stage, all patients received a DTI and PI scan. The single shot diffusion scan was always acquired preceding the perfusion scan. In addition, a MR angiographic (MRA) examination was performed at the initial time point to fully characterize any perfusion abnormality. All images were obtained using a 1.5T General Electric Medical systems (GEMS) Echospeed scanner with a maximum gradient strength of 23 mT/m. Due to individual working practices at each stroke clinic and upgrades of respective echoplanar imaging (EPI) protocols, three different DTI sequences were employed. Conventional fast spin echo T_2-weighted images were acquired at all time points. The total MRI examination time was within 20 min.

3. Diffusion tensor imaging (DTI)

Diffusion images for patients 1–9,18,19 were acquired with a spin-echo, echoplanar DTI sequence with the following acquisition, 18 axial slice full brain coverage, FOV = 30 cm, TR = 10s, TE = 105 ms, 5 mm slice thickness with

1 mm gap and 4 b-values per direction (6 gradient directions). The maximum b-value was 875 s mm^{-2}. The acquisition matrix was 128 $\times$ 144 (fractional Ky sampling) with a resulting image matrix of 256 $\times$ 256. Raw images were corrected for the presence of eddy current-induced warping artifacts. For patients 10–12, an optimized DTI sequence was employed [27]. Imaging parameters were 18 axial slices, FOV = 24 cm, TR = 6s, TE = 122 ms, 5 mm slice thickness with 1 mm gap and 28 b-values per direction [7 gradient directions, 25 high (b = 1112 s mm^{-2}) and 3 low b-values (b = 0)]. The acquisition matrix was 96 $\times$ 96 and the reconstruction matrix was 128 $\times$ 128. For patients 13–17, the imaging parameters for the DTI sequence were 15 axial slices, FOV = 24 cm, TR = 10s, TE = 120 ms, 5 mm slice thickness with 1.5 mm gap and 28 b-values per direction [7 gradient directions, 21 high (max 1220 s mm^{-2}) and 7 low b-values (b = 0)]. The acquisition matrix was 96 $\times$ 96 and the reconstruction matrix was 128 $\times$ 128. Isotropic diffusion weighted images were derived from the trace of the diffusion tensor as reported by Sorensen et al.[3] Diffusion metrics from these images were used in the normal classifier algorithm. Apparent diffusion coefficient (ADC) measures were not used in this study for automated extraction of lesion volumes or modeling infarct evolution due to potential problems associated with noise-floor effects in penumbral regions where there is inherent low signal intensity.

4. Perfusion imaging (PI)

Quantitative cerebral blood perfusion maps were obtained utilizing dynamic fast bolus tracking of GdDTPA (30 mL, Gd-diethylenetriaminepenta acetate "Magnevist," Schering, Germany) using a spin echo EPI sequence. The imaging parameters were for patients 1–9,18,19: 10 axial slices, FOV = 30 cm, image matrix = 128 $\times$ 128, TR = 1.85 s, TE = 60 ms, 7 mm slice thickness with 1 mm gap with acquisition of 50 frames per slice. For patients 10–12, 13 axial slices were acquired with FOV = 24 cm, image matrix 128 $\times$ 128, TR = 2.51 s, TE = 60 ms, 7 mm slice thickness with 1 mm gap with acquisition of 30 frames per slice. The imaging parameters for patients (13–17) were: 9 axial slices, FOV = 24 cm, TR = 1.85 s, TE = 60 ms, 7 mm slice with 2.5 mm gap with acquisition of 50 frames per slice. Baseline images were acquired for a period of 10 s, after which the contrast agent was injected with a Medrad Power Injector at 5 mL s^{-1}. Quantitative maps of CBF, CBV and MTT were calculated using the method described by Ostergaard et al. [17,28,29] To cover the entire penumbral territory the perfusion images were acquired with an increased slice thickness and slice gap compared to the DTI sequence. The perfusion maps were subsequently registered and re-sliced to the initially prescribed diffusion images using the methods described below. Ratio measures of perfusion (r$_a$CBF and r$_a$CBV) within the MTT territory were calculated relative to the contralateral hemisphere.

5. Image processing

5.1 Image registration and calculation of diffusion and perfusion metrics

Apart from the manual definition of a rectangular ROI around the MCA (via mouse control), an automated algorithm was used to define the optimum arterial input function prior to calculation of CBF maps. For every pixel within the described ROI a cubic spline was evaluated to model pixel signal as a function of time. The cubic spline function possessing the largest minima and the least signal fluctuation was then selected. The corresponding pixel was assigned as the MCA pixel which best represented the arterial input function. In this study, CBF maps were generated from arterial input functions defined from the MCA contralateral to the DWI lesion. Subsequent ultrasound evaluation of the carotid artery on the side used for the arterial input function did not reveal any stenosis greater than 50%. To enable registration of perfusion maps to diffusion images, raw spin-echo EPI perfusion images were coregistered to the initial T$_2$-weighted DWI scan (b = 0) using a 6 parameter rigid body transformation [30]. A similar transformation was also used to coregister serial diffusion scans. As FLAIR images [5] were not acquired in this study, the final lesion volume was derived after normalization and subtraction of initial T$_2$-weighted diffusion scans (b = 0) from follow-up DTI scans (b = 0). This enabled a more accurate delineation of the infarct volume as pixels with hyperintense signal originating from ventricular and sulcal cerebral spinal fluid (CSF) were excluded from the T2 lesion mask. An automated mid-plane algorithm was used to calculate diffusion and perfusion ratio measures between the infarcted and contralateral hemispheres. This algorithm comprised flipping the image in the Y plane followed by registration of the mirrored image to it's original form with a six parameter rigid body transformation [30]. The mid-plane was then determined by halving the resulting rotations and translations. Difference maps (e.g., dDWI and dMTT) for the ischemic territory were generated by the subtraction of corresponding voxels in the contralateral hemisphere. To aid delineation of the diffusion abnormality on the initial isotropically weighted diffusion image [3], a composite image was calculated from the product of the initial diffusion image and the dDWI map on a pixel-by-pixel basis. A bimodal *t* test was then performed on this image to create a binary diffusion mask. In a similar fashion, a MTT composite image was calculated by multiplication of the initial MTT map with the dMTT map and with the initial isotropically
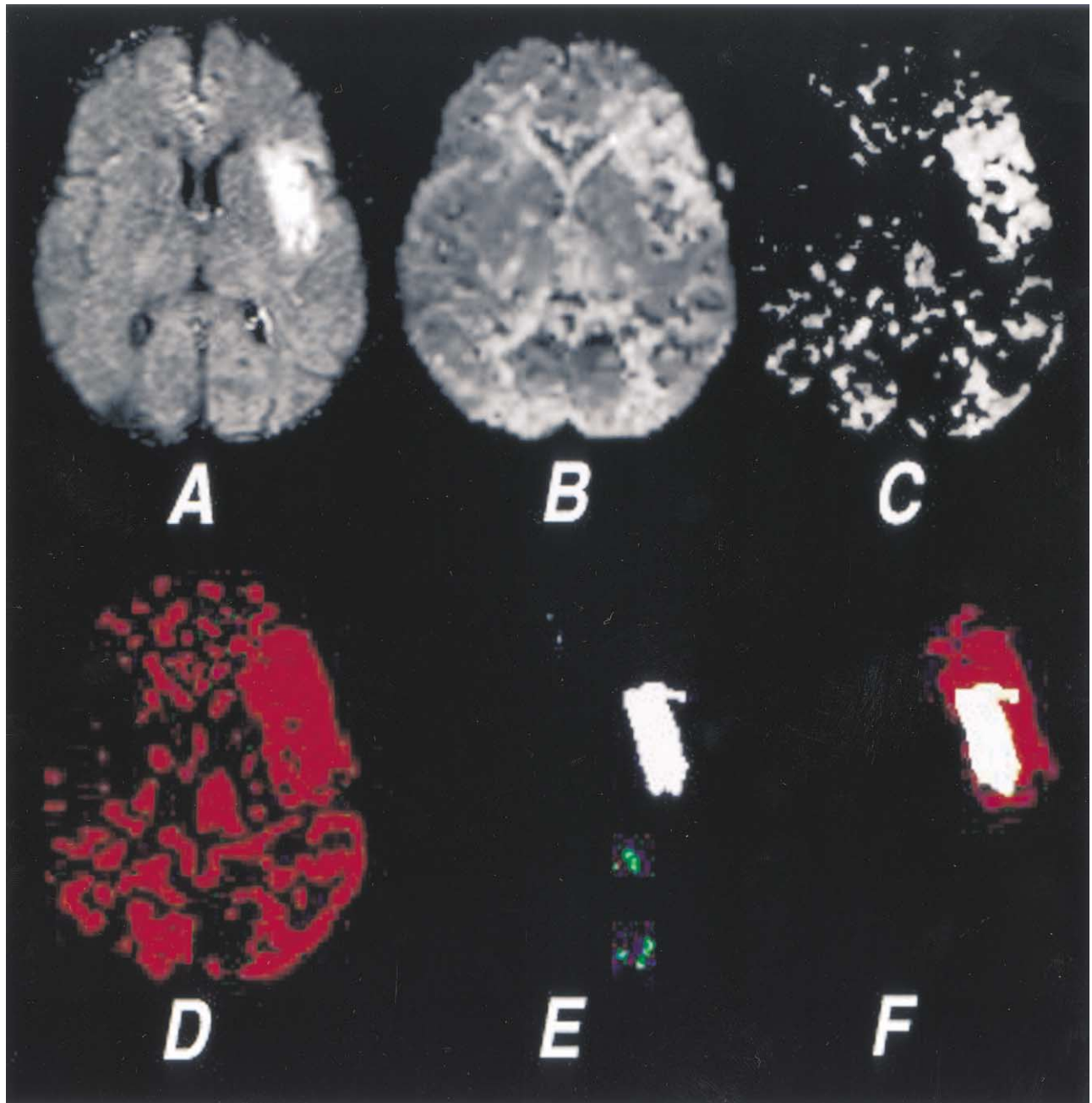
Fig. 1. Images representing automated extraction of the diffusion lesion and MTT ROI. From top left to top right, (A) the isotropically weighted diffusion image, (B) the corresponding registered MTT map and (C) the composite MTT map derived from the product of the initial diffusion image, MTT map and difference MTT map. The bottom images represent (D) the binary image of the composite MTT map, (E) the binary diffusion mask (green regions are artifacts removed from the mask) and (F) the binary MTT mask (red) extracted after initial seeding from the diffusion mask and application of the 3D region growing algorithm.

weighted diffusion image on a pixel-by-pixel basis. This yielded a MTT mask that was specific only to brain tissue as defined on the DWI scan. Using the DWI mask as the initial seed, a three dimensional region-growing technique [19] was then employed to extract the MTT mask from the composite MTT map. The task of extracting the MTT mask was simplified by only interrogating the hemisphere containing the ischemic lesion. Intermediate composite maps along with binary diffusion and MTT masks for a representative patient (subject 5) are given in Fig. 1. Absolute and ratio perfusion measures between the infarcted and contralateral hemispheres for three specific penumbral regions were interrogated. These three regions were the initial diffusion ROI, the territories within the MTT mask that went onto infarction and the tissue that survived the ischemic episode. Differences between perfusion measures for the three regions were tested with ANOVA.
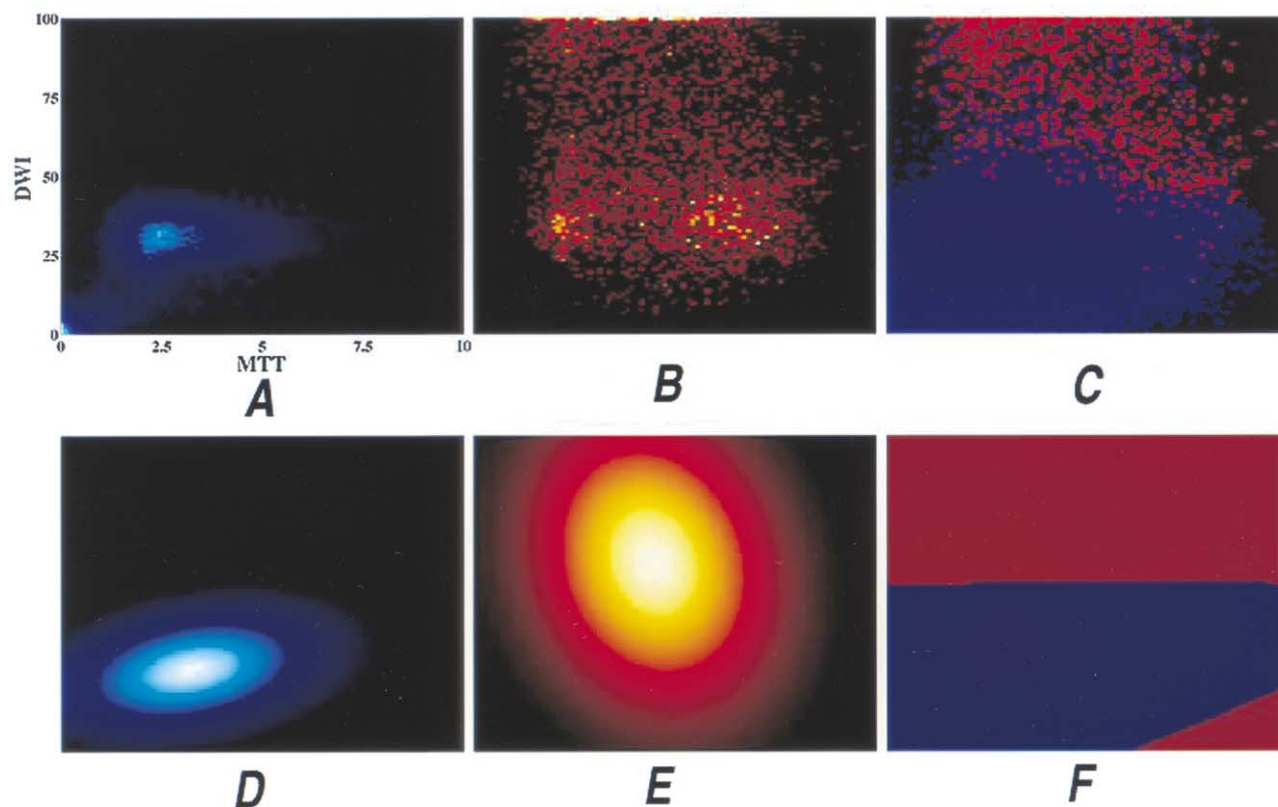
Fig. 2. The mechanics of the mixture model algorithm. Representative histograms plotting the isotropically weighted diffusion pixel intensity (arbitrary units) versus MTT measures were produced. From top left to top right, the histograms for all penumbral pixels which correspond to tissue which survived the ischemic event (A) and those within the final infarcted lesion volume (B) for a given patient are presented. The combined intensity profile for the two tissue types is given in (C). Bottom, left to right, (D) and (E) contain the normal functions modeling the frequency distributions of A and B, and (F) shows the resultant classification function.

6. Parametric normal classifiers

Parametric normal classifiers [26] were employed to predict the spatial location and size of the final lesion from diffusion and perfusion images acquired in the acute stage of stroke. Each pixel in the model was classified into two groups: those corresponding to the final T2 lesion, which are defined as infarcted, and those representing tissue that has survived the ischemic event. For the purpose of illustration, a model employing a parameter vector x-containing the diffusion and MTT pixel intensities was defined (see Fig. 2). Representative frequency histograms were produced where the isotropically weighted diffusion pixel intensity (arbitrary units) is plotted versus MTT measures for all pixels outside (histogram A, pixels color coded blue) and within the final lesion volume (histogram B, pixels color coded red). In 2(C), each histogram bin is classified into one of the two groups in accordance with the frequencies in histograms A and B. Mathematically, each group can be modeled by a normal distribution (f_i) with a mean parameter vector (μ_i) containing d parameters, covariance matrix (Σ_i) and prior probability (p_i) determined from the training data set using the following equation,[26]

$$f_i(x) = \frac{p_i}{(2\pi)^{d/2}|\Sigma_i|^{1/2}} \exp\left(-\frac{1}{2}(x - \mu_i)^T \Sigma_i^{-1}(x - \mu_i)\right)$$

(1)

The histograms A and B given in Fig. 2, were modeled by the normal distributions in histograms D and E, respectively. The model classifies each new pixel in accordance with the relative heights of the two group allocation functions:

$$g(x) = \arg\max_i f_i(x)$$

(2)

2(F) shows the resultant classification function. New pixels that fall within the red region would be allocated as destined to infarct, while those in the blue would be assigned as penumbral tissue that would survive the ischemic event. This methodology was employed using an eight-parameter vector (DWI, r_aDWI, CBF, r_aCBF, CBV, r_aCBV, MTT and r_aMTT) for all pixels within the MTT mask. Probability distributions were initially calculated from the data of ten patients (subjects 1–10). To validate the method, the model was then applied to seven novel patients (11–17). Each patient in the training data cohort was then considered individually. A model was determined from the remaining

Table 1
Summary of imaging results

Patient	Arterial territory	Time of first scan (hrs)	Acute volumes (ml)			Follow-up T2 (hrs)	Predicted volume (ml)	Measure of Accuracy			
			DWI	MTT	Mismatch			Sensitivity	Specificity	Positive predictive value	Negative predictive value
1	MCA+PCA	12	45.0	77.9	32.9	70.0 (111)	74.5	0.76	0.97	0.71	0.98
2	MCA_sv	13	6.3	14.7	8.4	11.5 (1290)	13.7	0.85	0.99	0.71	0.99
3	MCA_sv	13	13.0	15.6	2.6	14.9 (910)	15.4	0.66	0.99	0.64	0.99
4	MCA_sv	8	8.2	46.5	38.3	36.1 (749)	48.4	0.75	0.96	0.56	0.98
5	MCA_sv	11	10.8	28.9	18.1	27.8 (827)	28.8	0.75	0.98	0.74	0.98
6	MCA	13	9.5	48.5	39.0	56.9 (2160)	47.5	0.59	0.98	0.71	0.96
7	MCA_sv	12	3.3	34.6	31.3	23.1 (182)	37.7	0.83	0.94	0.51	0.99
8	MCA_sv	12	4.1	8.8	4.7	8.5 (2688)	8.2	0.69	0.99	0.80	0.99
9	MCA_sv	6	2.1	8.3	6.2	7.6 (1176)	8.2	0.80	0.99	0.74	0.99
10	MCA	2	2.7	169.5	166.8	167.1 (96)	168.8	0.69	0.95	0.69	0.95
11	MCA	4	70.9	168.9	98.0	148.9 (724)	163.4	0.80	0.95	0.73	0.97
12	MCA	3	25.7	142.7	117.0	134.2 (96)	137.9	0.66	0.94	0.64	0.94
13	MCA	7	75.9	146.0	70.1	146.2 (806)	137.8	0.69	0.95	0.73	0.94
14	MCA_sv	9	0.4	6.4	4.0	5.0 (678)	4.4	0.68	0.99	0.79	0.99
15	PCA	11	7.9	23.8	15.9	20.6 (691)	22.7	0.73	0.98	0.66	0.99
16	PCA	6	8.2	20.9	12.7	16.9 (720)	18.6	0.72	0.99	0.65	0.99
17	MCA	10	19.3	60.2	40.9	42.2 (738)	55.8	0.76	0.98	0.58	0.99
18*	MCA	10	13.6	210.0	196.4	117.8 (745)	199.4	0.71	0.88	0.42	0.96
19*	MCA	7	3.5	79.2	75.7	171.6 (151)	82.8	0.24	0.95	0.50	0.87
mean (1–10)								0.74	0.97	0.68	0.98
SD								0.08	0.02	0.09	0.01
mean (12–17)								0.72	0.97	0.68	0.97
SD								0.05	0.02	0.07	0.02
mean (12–19)								0.65	0.96	0.63	0.96
SD								0.17	0.04	0.12	0.04
mean (9–12, 16)								0.73	0.96	0.69	0.97
SD								0.06	0.02	0.05	0.02

* Serial MRA examinations revealed progressive occlusion of the MCA. MVA-sv denotes small vessel occlusion in the MCA territory.

nine patients and applied to the individual patient. The efficiency of prediction was given by measures of sensitivity, specificity, positive predictive value and negative predictive value [35].

7. Results

Patient demographic and imaging data are given in Table 1. Mean volumes of the automatically extracted diffusion lesion and MTT mask measured at the initial time point were 17.4 ± 21.7 and 69.0 ± 65.3 mL respectively. The mean follow-up final lesion volume measured from the T2 weighted DTI scan (b = 0) was 64.6 ± 59.5 mL. Perfusion measures derived from the automatically extracted masks are listed in Table 2. The mean r_aCBF and r_aCBV values for the ROI defined by the corresponding initial DWI lesion were 0.54 ± 0.19 and 1.02 ± 0.30. The mean r_aCBF and r_aCBV values for the entire infarcted territory within the MTT mask were 0.70 ± 0.19 and 1.20 ± 0.36. For recovered tissue within the MTT mask, the mean r_aCBF and r_aCBV values were 0.99 ± 0.25 and 1.87 ± 0.71 respectively. There was a significant difference between the initial diffusion ROI and recovered MTT territory for both of these

perfusion measures (both $p < 0.0001$). Comparison of the mean r_aCBF and r_aCBV values for tissue within the infarcted and recovered MTT masked territory also revealed significant differences between the two regions. The level of significance for the two measures were $p < 0.003$ and $p < 0.001$, respectively. As expected, the MTT territory that survived infarction exhibited the largest r_aCBF values.

For absolute perfusion measures, the mean CBF (ml/100g/min) and CBV (ml/100g) values for the corresponding initial DWI lesion were 26.6 ± 8.3 and 3.4 ± 1.2. The mean CBF and CBV values for the total infarcted territory were 33.9 ± 9.7 and 4.2 ± 1.9. For recovered tissue within the MTT mask, the mean CBF and CBV values were 41.5 ± 7.2 and 5.3 ± 1.2, respectively. For normal tissue, defined as tissue within the MTT mask reflected onto the contralateral hemisphere, the CBF and CBV values were 58.6 ± 14.7 (ml/100g/min) and 4.2 ± 1.4 (ml/100g/min), respectively. These values correlate to previously reported perfusion measures [32]. There was a significant difference between the initial diffusion ROI and recovered tissue within the MTT mask for both absolute perfusion measures ($p < 0.0001$). A significant difference was also found for the CBF and CBV values in the infarcted and recovered MTT regions, $p < 0.009$ and $p < 0.036$ respectively. The signif-

Table 2
Summary of perfusion imaging results

Patient	r_aCBF			CBF (ml/100g/min)				r_aCBV			CBV (ml/100g)			
	Initial DWI lesion	Infarcted tissue	Recovered tissue	Initial DWI lesion	Infarcted tissue	Recovered tissue	Normal tissue	Initial DWI lesion	Infarcted tissue	Recovered tissue	Initial DWI lesion	Infarcted tissue	Recovered tissue	Normal tissue
1	0.45	0.64	1.36	22.7	27.4	43.9	59.5	0.79	0.84	2.03	2.1	2.2	4.9	3.7
2	0.78	0.73	1.30	20.8	21.8	34.2	39.1	1.34	1.07	1.74	2.6	2.5	3.6	3.2
3	0.63	0.77	1.03	26.3	34.2	44.9	49.2	0.89	0.88	1.31	2.5	2.8	4.4	3.7
4	0.43	0.68	0.88	20.2	34.5	42.3	55.9	1.29	1.89	2.24	3.5	5.6	6.8	3.3
5	0.41	0.62	1.23	33.3	43.0	46.0	83.2	0.94	1.07	1.75	4.6	5.0	6.3	5.6
6	0.73	0.99	1.10	26.5	32.2	30.2	39.6	1.42	1.77	2.80	4.9	6.1	6.1	3.9
7	0.64	0.77	0.95	39.2	52.9	48.2	76.6	1.29	1.63	1.73	5.5	8.0	6.3	5.4
8	0.69	0.87	1.15	33.5	38.0	47.5	53.0	1.11	1.21	1.42	3.7	3.6	3.9	3.7
9	0.79	0.84	0.92	23.9	27.2	32.0	38.2	1.38	1.37	1.31	3.0	3.5	2.8	3.0
10	0.39	0.71	0.71	28.6	35.3	34.3	59.0	0.72	1.51	1.54	3.3	4.3	4.2	3.2
11	0.33	0.48	0.94	18.7	24.7	48.6	58.0	0.67	0.86	1.79	2.5	3.1	6.8	4.0
12	0.26	0.60	0.81	13.9	23.1	33.2	51.8	0.58	1.12	1.78	2.4	3.7	5.8	4.0
13	0.23	0.34	0.56	16.2	24.1	38.1	79.0	0.46	0.57	1.38	1.9	2.6	6.1	5.1
14	0.58	0.67	0.73	34.7	49.8	45.8	79.8	0.78	1.07	1.06	5.9	9.0	6.8	8.6
15	0.56	0.46	0.64	24.4	26.3	40.1	71.4	0.91	0.75	1.07	2.7	3.2	5.5	6.0
16	0.45	0.64	1.35	15.9	25.8	31.8	39.3	0.91	1.02	4.15	2.4	2.8	4.2	2.8
17	0.39	0.49	0.81	26.3	32.8	54.7	71.5	1.31	1.41	2.48	2.7	3.1	6.1	2.5
18	0.80	1.00	1.18	43.1	39.8	44.4	49.5	1.36	1.57	2.07	4.9	4.5	4.9	3.5
19	0.79	1.05	1.25	37.2	50.9	48.8	59.3	1.16	1.24	1.94	3.6	4.4	5.5	4.0
mean	0.54	0.70	0.99	26.6	33.9	41.5	58.6	1.02	1.20	1.87	3.4	4.2	5.3	4.2
SD	0.19	0.19	0.25	8.3	9.7	7.2	14.7	0.30	0.36	0.71	1.2	1.9	1.2	1.4

Note: Infarcted tissue represents brain tissue within the MTT mask that went onto infarction and recovered tissue represents tissue within the MTT mask that survived the ischemic event.

icance level for the difference in CBF values for normal and recovered tissue was $p < 0.0001$. In contrast, the cerebral blood volume was increased in this important penumbral territory ($p < 0.011$). Hypervolemia in the ischemic penumbra, measured using MR dynamic bolus tracking has previously been reported [16,21,31].

Measures of efficiency of the predictive model are given in Table 1. We found that an 8 dimensional model utilizing the metrics r_aDWI, DWI, r_aMTT, MTT, r_aCBF, CBF, r_aCBV and CBV gave optimal predictive efficiency. Independent use of only ratio or absolute diffusion and perfusion values, significantly reduced the measures of sensitivity and positive predictive value. The mean measures of sensitivity, specificity, positive predictive value and negative predictive value for the training data sets (patients 1–10) were 0.74 ± 0.08, 0.97 ± 0.02, 0.68 ± 0.09 and 0.98 ± 0.01, respectively. For the validation data sets (patients 11–17) the values were 0.72 ± 0.05, 0.97 ± 0.02, 0.68 ± 0.07 and 0.97 ± 0.02, respectively. The measures of predictive efficiency including results for both subjects (18,19) who presented with progressive occlusion of the MCA, found on serial MRA examinations, were 0.65 ± 0.17, 0.96 ± 0.04, 0.63 ± 0.12 and 0.96 ± 0.04, respectively. The measures of predictive efficiency for the five subjects (9–12,16) scanned within six hours of onset of symptoms were 0.73 ± 0.06, 0.96 ± 0.02, 0.69 ± 0.05 and 0.97 ± 0.02, repectively.

Diffusion and perfusion maps together with predicted infarct territories for two representative patients are given in Figs. 3 and 4. These images show an arbitrary mid-stroke slice for patients belonging to the training data cohort (Patient 10, Fig. 3) and validation data set (Patient 17, Fig. 4), respectively. The extracted MTT masks are colored blue with the corresponding predicted infarct territory colored red. For Patient 10, 2 h after onset of symptoms (Fig. 3), the MRA shows an occlusion of the left MCA along with a small, poorly defined diffusion lesion in deep white matter of the MCA territory with a corresponding large MTT abnormality. The MTT map revealed areas of reduced CBF and increased CBV. Although there is some evidence of edema on the follow-up T2 weighted image, there is a close correlation between the predicted lesion size and the T2 defined infarct volume. In this hyperacute case the model correctly predicted that the infarct would grow into the entire hypoperfused territory even though the MTT region contained predominantly hypervolemic tissue. In comparison, the images of Patient 17 shown in Fig. 4, acquired 10 h after onset of symptoms, reveal a well-defined DWI lesion resulting from occlusion of the left MCA. The large MTT abnormality shows regions of reduced CBF and a heterogeneous pattern of both reduced and elevated CBV. In this case, where data were acquired 10 h after onset of symptoms, the model correctly predicted infarct evolution into the MTT territory. As can be seen in Table 1, the volume of the extracted MTT masks for patients in this study correlated with the final lesion volume ($r = 0.88$). The mean MTT mask and final lesion volumes were 69 ± 65.3 and
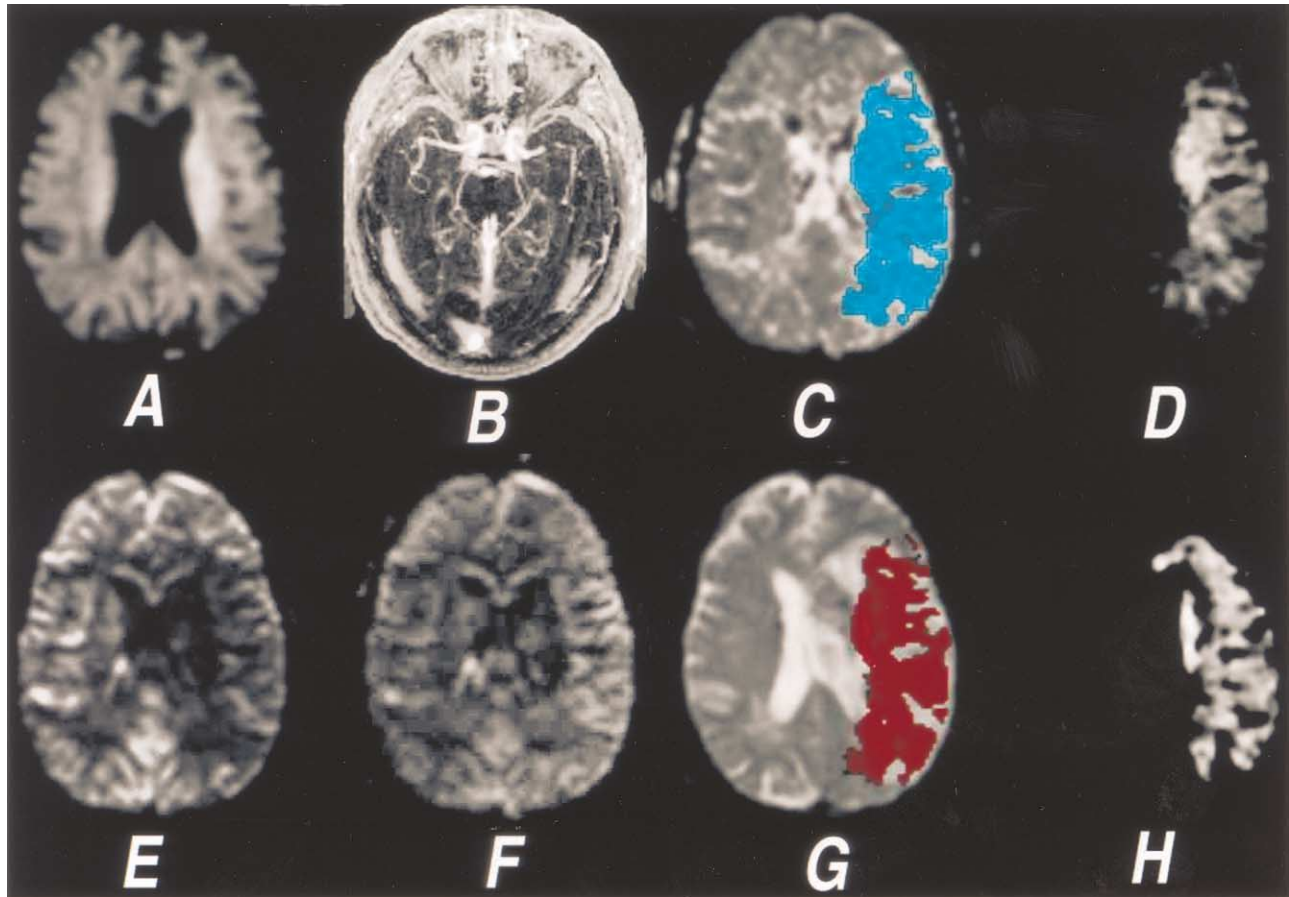
Fig. 3. Diffusion and perfusion images acquired for a representative patient from the training data sets (Patient 10), two hours after onset of symptoms. Top, left to right, (A) the DWI scan showing a poorly defined diffusion lesion in the deep white matter in the left hemisphere, (B) the MRA showing occlusion of the left MCA, (C) the MTT map with the extracted MTT mask given in blue and (D) the composite MTT map. Bottom left to right, (E) CBF, (F) CBV, (G) the follow-up T$_2$-weighted scan (b = 0) with predicted lesion colored red and (H) the final lesion volume derived by subtraction of the initial T2 image from the follow-up scan.

64.6 ± 59.5 mL. This correlation demonstrates that for this group of subjects the extracted masks correctly identified tissue with an altered hemodynamic function. The computational time, including calculation and registration of DWI and PI maps and modeling of infarct evolution was less than 10 min using a Silicon Graphics Octane workstation.

8. Discussion

In this study, we have introduced a strategy to automatically extract masks of the diffusion lesion and regions of abnormal hemodynamic function defined on MTT maps acquired in the acute stage of stroke. This methodology allows rapid assessment of diffusion, CBF, CBV and MTT measures within the MTT mask, including the diffusion–perfusion mismatch and estimation of infarct evolution using predictive modeling techniques. Recent studies have redefined the relationships between the ischemic penumbra and diffusion and perfusion abnormalities seen on MR imaging [22]. The predictive modeling strategy reported in this

study does not depend upon the identification of an ischemic penumbra. This methodology may prove useful for patient assessment prior to possible therapeutic intervention and importantly in the analysis of data from large clinical stroke trials.

Surprisingly few studies have been published in the literature reporting MR-derived perfusion measures within the penumbral territory in humans [16,23,31–33,39]. Many of these studies have relied on the use of manually defined ROIs on perfusion images and therefore contain additional information from non-brain tissue from ventricular or sulcal regions. Our data extends previous results by (i) utilizing voxel based perfusion analyses from only brain tissue and (ii) including absolute measures of blood flow and blood volume in the MTT territory from both infarcted tissue and tissue which survived the ischemic event.

In the territory of the MTT mask, we found a significant decrease in r$_a$CBF (0.70 ± 0.19) and CBF (33.9 ± 9.7 mL/100g/min) in tissue that went onto infarction compared with tissue which survived the ischemic event (0.99 ± 0.25 and 41.5 ± 7.2 mL/100g/min, respectively). The r$_a$CBF
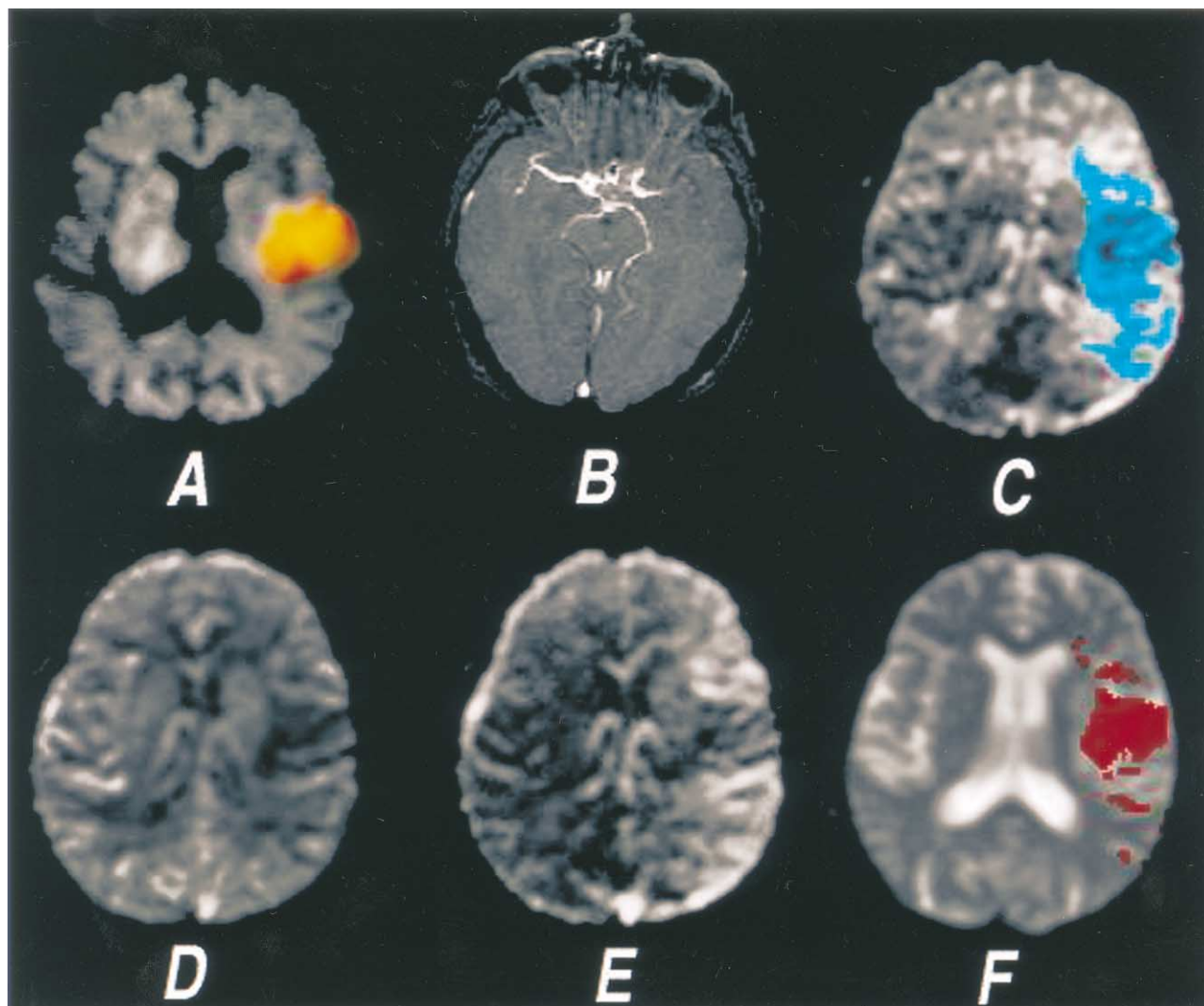
Fig. 4. Diffusion and perfusion images acquired for a representative patient from the validation data sets (Patient 17), ten hours after onset of symptoms. Top left to right, (A) the DWI scan showing a diffusion lesion in the left MCA territory (diffusion mask colored orange), (B) the MRA showing occlusion of the left MCA, and (C) the MTT map with extracted MTT mask given in blue. Bottom left to right, (D) CBF, (E) CBV and (G) the follow-up T_2-weighted scan (b = 0) with predicted lesion colored red.

values calculated in our study are very similar to those reported from SPECT studies [34] namely, 0.48 ± 0.10 and 0.75 ± 0.10 for the ischemic core and penumbra respectively. Quantitative CBF measures in the the initial DWI lesion and diffusion-perfusion mismatch territory of 34.4 ± 22.4 and 50.2 ± 17.5 (ml/100g/min) have been reported in stroke patients [33]. Although these values are similar to those measured in our study, no distinction was made in that study between tissue that survived or went onto infarction in the MTT territory. In the group of patients investigated in this current study, quantitative measures of CBF were reduced in all regions of the MTT territory compared with normal tissue on the contralateral side. This included tissue within the MTT mask that recovered or eventually progressed to infarction. An analogous result has been reported previously [33]. In five of the nineteen patients there was increased CBF in the diffusion–perfusion mismatch region

which progressed to infarction, as defined on the follow-up T2 weighted scan (patients 6,7 10,14 and 19). In our investigation, this observation was not apparent in contralateral ratio measures. This finding highlights an advantage of measuring absolute rather than ratio perfusion measures within the MTT ROI. The accuracy of ratio measures relies on a number of factors. These include (i) symmetrical brain morphology, (ii) the bilateral absence of pathologic processes such as white matter disease, and (iii) head positioning in the scanner so that the brain appears symmetrical in the sagittal plane. Although the underlying pathophysiological reason for this observation is unclear, a possible mechanism may involve collateral flow to leptomeningeal vessels already undergoing vasodilation due to an altered hemodynamic function or a process involving increased flow via anastamotic vessels to a hypoperfused region. The finding of increased penumbral blood flow has been reported by others

using both ratio measures [16] and quantitative arterial spin labeling methods [33]. The diffusion–perfusion mismatch regions with increased CBF correlated with tissue exhibiting enhanced CBV. Such a correlation gives evidence of a possible mechanism involving vasodilation of collateral leptomeningeal vessels [16]. This highlights the fact that within the MTT territory, tissue that survives the ischemic event is not always restricted to regions with increased cerebral blood flow.

Patients in our study exhibited a heterogeneous pattern of both reduced and elevated cerebral blood volume measures within the MTT mask. Penumbral tissue with increased measures of CBV have been reported in other studies [16, 22,31]. Elevated CBV measures have been shown not to result from a breakdown of the blood-brain barrier and leakage of Gd-DTPA [31] but to vasodilation of leptomeningeal vessels in response to an altered hemodynamic state to maintain cerebral perfusion pressure [36]. Due to the diverse nature of CBV values in the MTT mask in the present study, predicting infarct evolution utilizing threshold levels of this metric may have limited use. In humans, the modeling of stoke evolution is a complex problem because of the limited information that can be obtained in vivo regarding some of the important underlying mechanisms believed to be involved with neuronal death. Thus we are using diffusion and perfusion imaging as surrogate markers to model and predict complex pathophysiological processes such as apoptosis, that occur following an ischemic episode [37,38]. However, given these constraints we have demonstrated that diffusion and perfusion measures acquired in the acute phase of stroke can be used to model infarct evolution. Although the time of first scan after onset of symptoms was 8.9 ± 3.5 h we found that exclusion of the diffusion metrics did not reduce the model's predictive power. The measures of sensitivity, specificity, positive predictive value and negative predictive value for the validation data sets derived using only the perfusion metrics were 0.72 ± 0.05, 0.97 ± 0.02, 0.67 ± 0.07 and 0.97 ± 0.02, respectively. Furthermore, for the five patients (9–12,16) who were scanned within the six hour window after onset of symptoms the measures of predictive efficiency were of similar magnitude, namely 0.73 ± 0.06, 0.96 ± 0.02, 0.69 ± 0.05 and 0.97 ± 0.02, respectively. This suggests that this methodology may be suitable for hyperacute stroke patients ($<$6 h after onset of symptoms) which present with large diffusion- perfusion mismatches. With this strategy, we assume that the MTT mask represents the boundary for possible infarct evolution. It is possible with this methodology for the predicted lesion to be slightly larger than the calculated MTT mask. Such a result can be seen in three patient's data (see Table 1, patients 4,7,19). This anomaly can arise when the diffusion mask is not spatially congruent with the MTT mask, i.e., a portion of the diffusion mask lays outside of the MTT masked region. This problem can occur when registration of the diffusion and perfusion images is compromised because of head movement or the presence of artifacts within the diffusion image.

In this study, we routinely used the contralateral MCA to define the arterial input function for the calculation of perfusion maps. In using this vessel we assume that there is little or no concurrent carotid stenosis or occlusion that may affect the accuracy of resulting perfusion maps. Two patients (5,10) possessed moderate contralateral stenoic carotid arteries (50–75%) and one (19) had significant occlusion (80–90%). Although the predictive model was accurate for both patients (5,10), further work is required to fully determine the correlation between concurrent carotid stenosis and model efficiency. In addition, a larger subject cohort may also enable identification of distinctive angiographic and perfusion characteristics that allow recognition of acute stroke patients who present with progressive occlusion of the MCA. Such patients with dynamically evolving lesions are a future challenge for predicting infarct growth.

In conclusion, we have endeavored to introduce a strategy to automatically extract diffusion and MTT masks from diffusion and perfusion images acquired in the acute phase of stroke. In contrast to manually drawn ROIs, the automatically extracted perfusion masks used in this study contain hemodynamic information from only brain tissue and thus may better characterize measures of CBF and CBV within the MTT territory. For this reason we have purposely avoided comparing results derived from manually traced ROIs. Furthermore, we have shown that diffusion and perfusion measures defined by these masks can be modeled to predict stroke evolution. Clearly this model needs to be applied to a much larger data set to prove validity of the strategy.

Acknowledgments

References

[1] Warach S, Chien D, Li W, Ronthal M, Edelman RR. Fast magnetic resonance diffusion–weighted imaging of acute human stroke. Neurology 1992;42:1717–23.

[2] Warach S, Gaa J, Siewert B, Wielopolski P, Edelman RR. Acute human stroke studied by whole brain echo planar diffusion- weighted magnetic resonace imaging. Ann Neurol 1995;37:231–41.

[3] Sorensen AG, Buonanno FS, Gonzalez RG, Schwamm LH, Lev MH, Huang-Hellinger FR, Reese TG, Weisskoff RM, Davis TL, Suwanwela N, Can U, Moreira JA, Copen WA, Look RB, Finklestein SP, Rosen BR, Koroshetz WJ. Hyperacute stroke: evaluation with combined multisection diffusion- weighted and hemodyamically weighted echo-planar MR imaging. Radiology 1996;199:391–401.

[4] Schlaug G, Siewert B, Benfield A, Edelman RR, Warach S. Time course of the apparent diffusion coefficient (ADC) abnormality in human stroke. Neurology 1997;49:113–9.

[5] Beaulieu C, de Crespigny A, Tong DC, Moseley ME, Albers GW, Marks MP. Longitudinal magnetic resonance imaging study of perfusion and diffusion in Stroke: Evolution of Lesion Volume and Correlation with Clinical Outcome. Ann Neurol 1999;46:568–78.

[6] Busza AL, Allen KL, King MD, van Bruggen N, Williams SR, Gadian DG. Diffusion-weighted imaging studies of cerebral ischemia in gerbils: potential relevance to energy failure. Stroke 1992;23:1602–12.

[7] Mintorovitch J, Yang GY, Schimizu H, Kucharczyk J, Chan PH, Weinstein PR. Diffusion-weighted magnetic resonace imaging of acute focal cerebral ischemia: comparison of signal intensity changes in brain water, and Na(+)-K(+) ATPase activity. J Cereb Blood Flow Metab 1994;14:332–6.

[8] Back T, Hoehn-Berlage M, Kohno K, Hossmann KA. Diffusion nuclear magnetic resonance imaging in experimental stroke: correlation with cerebral metabolites. Stroke 1994;25:494–500.

[9] Zelaya F, Flood N, Chalk JB, Wang D, Doddrell DM, Strugnell W, Benson M, Ostergaard L, Semple J, Eagle S. An evaluation of the time dependence of the anisotrophy of the water diffusion tensor in acute human ischemia. Magn Reson Imaging 1999;17:331–48.

[10] Basser PJ, Pierpaoli CJ. Microstructural and physiological features of tissue elucidated by quantitative diffusion tensor MRI. J Magn Reson [B] 1996;111:209–19.

[11] Pierpaoli CJ, Jezzard P, Basser PJ, Barnett A, Di Chiro G. Diffusion tensor MR imaging of the human brain. Radiology 1996;201:637–48.

[12] Warach S, Dashe JF, Edelman RR. Clinical outcome in ischemic stroke predicted by early diffusion-weighted and perfusion magnetic resonance imaging. A preliminary analysis. J Cereb Blood Flow Metab 1996;16:53–9.

[13] Barber PA, Darby DG, Desmond PM, Yang Q, Gerraty RP, Jolley D, Donnan GA, Tress BM, Davis SM. Prediction of stroke outcome with echoplanar perfusion- and diffusion-weighted MRI. Neurology 1998;51:418–26.

[14] Tong DC, Yenari MA, Albers GW, O'Brien M, Marks MP, Moseley ME. Correlation of perfusion- and diffusion-weighted MRI with NIHSS score in acute (<6.5 h) ischemic stroke. Neurology 1998;50:864–70.

[15] Rordorf G, Koroshetz WJ, Copen WA, Cramer SC, Schaefer PW, Budzik RF, Schwamm LH, Buonanno F, Sorensen AG, Gonzalez G. Regional ischema and ischemic injury in patients with acute middle cerebral artery stroke as defined by early diffusion-weighted and perfusion- weighted MRI. Stroke 1998;29:939–43.

[16] Sorensen AG, Copen WA, Ostergaard L, Buonanno F, Gonzalez RG, Rordorf G, Rosen BR, Schwamm LH, Weisskoff RM, Koroshetz WJ. Hyperacute Stroke: Simultaneous measurement of relative cerebral blood volume, relative cerebral blood flow, and mean tissue transit time. Radiology 1999;210:519–27.

[17] Ostergaard L, Johannsen P, Host-Poulsen P, Vestergaard-Poilsen P, Asboe H, Gee AD, Hansen S, Cold G, Gjedde A, Gyldensted C. Cerebral blood flow measurements by magnetic resonance imaging bolus tracking: Comparison with [^{15}O] H$_2$O Positron emission tomography in humans. J Cereb Blood Flow Metab 1998;18:935–40.

[18] Sakoh M, Rohl L, Gyldensted C, Gjedde A, Ostergaard L. Cerebral blood flow and blood volume measured by magnetic resonance imaging bolus tracking after acute stroke in pigs. Comparison with [^{15}O] H$_2$O positron emission tomography. Stroke 2000;31:1958–64.

[19] Russ JC. The image processing handbook. (3rd ed.) Boca Raton, FL: CRC Press, 1999.

[20] Baird AE, Benfield A, Schlaug G, Siewart B, Lovblad KO, Edelman RR, Warach S. Enlargement of human cerebral ischemic lesion volumes measured by diffusion-weighted magnetic resonance imaging. Ann Neurol 1997;41:581–9.

[21] Schwamm LH, Koroshetz WJ, Sorensen AG, Wang B, Copen WA, Budzik R, Rordorf G, Buonanno FS, Schaefer PW, Gonzalez RG. Time course of lesion development in patients with acute stroke: serial diffusion- and hemodynamic-weighted magnetic resonance imaging. Stroke 1998;29:2268–76.

[22] Kidwell CS, Saver JL, Mattiello J, Starkman S, Vinuela F, Duckwiler G, Gobin P, Jahan R, Vespa P, Kalafut M, Alger JR. Thrombolytic reversal of acute human cerebral ischemic injury shown by diffusion/perfusion magnetic resonance imaging. Ann Neurol 2000;47:462–69.

[23] Schlaug G, Benfield A, Baird AE, Siewert B, Lovblad KO, Parker RA, Edelman RR, Warach S. The ischemic penumbra. Operationally defined by diffusion and perfusion MRI. Neurology 1999;53:1528–37.

[24] Wu O, Koroshetz WJ, Østergaard L, Ferdinando S, Buonano F, Copen WA, Gonzlez RG, Rordorf G, Rosen BR, Schwamm L, Weisskoff RM, Sorensen AG. Predicting tissue outcome in acute human cerebral ischemia using combined diffusion- perfusion-weighted MR imaging. Stroke 2001;32:933–42.

[25] Clark WM, Wissman S, Albers GW, Jhamandas JH, Madden KP, Hamilton S, et al. Recombinant tissue-type plasminogen activator (Alteplase) for ischemic stroke 3 to 5 hours after symptom onset. The ATLANTIS Study: A randomized controlled trial. JAMA 1999;282:2019–26.

[26] McLachlan GJ, Basford KE. Mixture models: inference and application to clustering. New York: Marcel Dekker, 1998.

[27] Jones DK, Horsfield MA, Simmons A. Optimal strategies for measuring diffusion in anisotropic systems by magnetic resonance imaging. Magn Reson Med 1999;42:515–25.

[28] Ostergaard L, Weisskoff RM, Chesler DA, Gyldensted C, Rosen B. High resolution measurement of cerebral blood flow using intravascular tracer bolus passages. Part I: mathematical approach and statistical analysis. Mag Reson Med 1996;36:715–25.

[29] Ostergaard L, Sorensen AG, Kwong K, Weisskoff RM, Gyldensted C, Rosen BR. High resolution measurement of cerebral blood flow using intravascular tracer bolus passages. Part II: experimental comparison and preliminary results. Mag Reson Med 1996;36:726–36.

[30] Collins DL, Neelin P, Peters TM, Evans AC. Automatic 3-D inter-subject registration of MR volumetric data in standardized Talairach space. J. Comput. Assis. Tomogr 1994;18:192–205.

[31] Hatazawa J, Shimosegawa E, Toyoshima H, Ardekani B, Suzuki A, Okudera T, Miura Y. Cerebral blood volume in acute brain infarction. A combined study with dynamic susceptibility contrast MRI and. 99m Tc-HMPAO-SPECT Stroke 1999;30:800–806.

[32] Smith AM, Garndin CB, Duprez T, Mataigne F, Cosnard G. Whole brain quantitative CBF, CBV and MTT measurements using MRI bolus tracking: Implementation and application to data acquired from hyperacute stroke patients. J Magn Reson Imaging 2000;12:400–10.

[33] Chalela JA, Alsop DC, Gonzalez-Atavales JB, Maldjian JA, Kasner SE, Detre JA. Magnetic Resonance perfusion imaging in acute ischemic stroke using continuous arterial spin labeling. Stroke 2000;31:680–7.

[34] Shimosegawa E, Hatazawa J, Inugami A, Fujita H, Ogawa T, Aizawa Y, Kanno I, Okudera T, Uemura K. Cerebral infarction within six hours of onset: prediction of completed infarction with technetium-99m-HMPAO SPECT. J Nucl Med 1994;35:1097–103.

[35] Sackett DL, Haynes RB, Guyatt GH, Tugwell P. Clinical epidemiology: a basic science for clinical medicine. (2nd ed.) Boston, MA: Little, Brown, and Company, 1991. pp. 79–110.

[36] Ferrari M, Wilson DA, Hanley DF, Traystman RJ. Effects of graded hypotension on cerebral blood flow, blood volume and mean transit time in dogs. Am J Physiol 1992;262H:1908–14.

[37] Du C, Hu R, Csernansky CA, Hsu CY, Choi DW. Very delayed infarction after mild focal cerebral ischemia: a role for apoptosis? J Cereb Blood Flow Metab 1996;16:195–201.

[38] Vexler ZS, Roberts TP, Bollen AW, Derugin N, Arieff AI. Transient cerebral ischemia. Association of apoptosis induction with hypoperfusion. J Clin Invest 1997;99:1453–9.

[39] Rohl L, Østergaard L, Simonsen CZ, Vestergaard-Poulsen P, Andersen G, Sakoh M, Le Bihan D, Gyldensted C. Viability thresholds of ischemic penumbra of hyperacute stroke defined by perfusion-weighted MRI and apparent diffusion coefficient. Stroke 2001;32:1140–6.